Modelling of liquid injection of ammonia in a direct injector using Reynolds-averaged Navier–Stokes simulation

Jessica Gaucherand[a,*], Corinna Netzer[a], Michał T. Lewandowski[a], Terese Løvås[a]

[a] *Department of Energy and Process Engineering, Norwegian University of Science and Technology (NTNU), Kolbjørn Hejes vei 1a, Trondheim, 7491, Trøndelag, Norway,*
jessica.gaucherand@ntnu.no

Abstract

Ammonia as a fuel has gotten attention in the past years to enable decarbonization for internal combustion engines. There is a need to understand the behavior of the liquid fuel in direct injection engines, a crucial step of the engine cycle. Injection impacts the mixture formation in the cylinder, equivalence ratio, combustion and pollutants formation. Liquid ammonia is expected to behave significantly different than traditional fuels during the injection phase and hence requires to be investigated. Indeed, recent experimental research has highlighted the appearance of flash boiling during injection of ammonia spray under engine-relevant conditions. The high volatility is also expected to influence the cavitation behavior. Cavitation is the partial vaporization of the liquid typically caused by locally increased velocity resulting in a pressure drop, when the fluid enters an orifice with sharp edges. One parameter controlling cavitation is therefore the geometry, but cavitation is also influenced by the fuel's property and the boundary conditions. This study presents 3-D RANS simulations performed with CONVERGE CFD of the internal flow of a Gasoline Direct Injector (GDI), operating with liquid ammonia. The transient simulations account for the injector needle movement. Simulations capture the presence of both vapor and liquid in the nozzle head. These results from the simulations will provide input data for separate spray simulations with the same engine geometry, as well as support the development of a 0-D model that will be important for design purposes. Preliminary results predict a liquid discharge coefficient of less than 0.1 at the outlet for injection in atmospheric conditions.

1. Introduction

Reduction of greenhouse gas emissions to mitigate climate change requires a change for the transportation sector both in the form of vehicles electrification or towards the usage of carbon-free fuels for internal combustion engines (ICE). Ammonia (NH_3) is one of the fuels of interest and has been investigated as a promising fuel for internal combustion engines (Lhuillier et al., 2020; Mounaïm-Rousselle et al., 2022): it can be stored in liquid form at an ambient temperature at 9 bar, has a high hydrogen content and no carbon. However, the fuel characteristics are very different from conventional fuels, including its behaviour in the injection system. The fuel injection in the engine is an important process deciding on mixture formation, equivalence ratio, combustion, and pollutant formation. So far the majority of ammonia applications in ICE have been performed with port injection, with the fuel in gaseous phase, leading to purely premixed combustion (Mounaïm-Rousselle et al., 2021; Niki et al., 2016). On the other hand, direct liquid ammonia injection allows for other combustion modes with more strategies to explore and can potentially reduce ammonia slip (unburned ammonia in the exhaust) (Reiter and Kong, 2008). In other words, studying the injection of liquid ammonia is of interest to optimize internal combustion engine performances and emissions with this fuel. There is little literature on ammonia sprays relevant for engine conditions, yet recent experimental works (Pelé et al., 2021; Cheng et al., 2022) shed some light on this topic. To gain further insights, numerical investigations of fuel in-nozzle flow allows to compare the fuel's behavior during injection, capture phase change in the injector (Torelli et al., 2017), and study spray formation in the engine (Saha et al., 2017).

This study aims to investigate numerically the internal flow of liquid ammonia in a gasoline direct injector (GDI). GDIs, which are solenoid activated injectors for high-pressure direct injection, are used in ICEs as they allow rapid response, increased engine efficiency, and reduced emissions (Wang et al., 2014). The flow travels throughout the injector due to a strong pressure gradient between the fuel system, where the fuel is stored at high pressure, and the engine's combustion chamber. The injector's internal geometry, the nozzle material, the tank and engine pressure and temperature, and the fuel's property affect the fluid flow. It is therefore expected that the fuel arriving at the injector's outlet will not have the same properties as in the tank. In particular, the sharp edges of the injector's nozzle hole cause a large pressure drop inducing vapor formation in the injector if the pressure drops below the saturation pressure of the fuel. This phenomenon is called cavitation. Cavitation can be destructive as a vapor bubble can collapse under high pressure and create a shockwave that can damage the nozzle material. Flash boiling denotes a condition where liquid undergoes a rapid pressure reduction and partial vaporization occurs due to the fuel's property and local pressure and temperature. These conditions occur during

spray formation in the combustion chamber but may also happen inside the injector during the injection: the latter phenomenon is referred to as internal flash boiling. Therefore, two sources of energy can be the cause for fuel vapor formation inside an injector : kinetic energy, or heating of the fuel. Studying the fuel's evolution, and more specifically its interaction with the injector needle motion and the nozzle holes, will provide useful inputs on the thermodynamic state of the fuel when it is injected into the engine. Previous research has been carried out with various fuels such as diesel or biodiesel, showing that each fuel behaves differently and cavitates at varying degree in identical injectors due to their physical properties (Torelli et al., 2017). Experiments have shown that in-nozzle flow cavitation for traditional fuels impact spray formation (Serras-Pereira et al., 2010). However, it remains unknown how ammonia behaves during the injection and how this contributes to the untypical ammonia spray characteristics observed in a recent studies (Pelé et al., 2021). This forms the motivation for the present work to gain further insights by looking at the internal flow of ammonia inside of an injector numerically. Additionally, the obtained results will be needed in future work for two purposes: as valuable information and input data for Lagrangian spray setup in separate simulations in similar ICE configurations; and to support the development of a 0-D model that can be used during design process of new and optimised injectors.

First, the numerical setup will be outlined with the description of the model equations, the injector's geometry, and a mesh convergence study. Then in the second part of the paper, results will be discussed with a focus on the flow characteristic at the injector's outlet. A comparison with iso-octane will also be presented. Finally, parameters such as the output pressure, the wall temperature will be modified to see the impact on the injection.

2. CFD setup and mesh study

In this work, a six-hole counter bore GDI fuel injector with ammonia is investigated. The geometry of the injector was obtained using molds of the physical injector and measurements conducted with a scanning electron microscope. The 3-D CFD simulations are carried out using the software CONVERGE 3.0 (Richards et al., 2017) within the Reynolds-averaged Navier Stokes (RANS) framework. The Navier Stokes solver is set to Pressure Implicit with Splitting of Operator algorithm (PISO). The simulation is transient with automatically adapted variable time step. The adaptative mesh refinement as allowed with CONVERGE is used to capture the fine nozzle details and the flow around the needle as it moves. The needle in the injector moves to open and close the passage of the fluid at the nozzle head. Turbulence is modeled with a Re-Normalization group (RNG) k-ϵ model. For the sake of brevity, details of the models are not discussed here.

2.1. Multi-phase flow model

To capture the effect of cavitation in the injector, a multi-phase approach is needed to describe both liquid and vapor flow and the interactions between the two. In this work, this is done using the volume of fluid (VOF) method. The liquid phase is represented with the subscript l, and the gaseous phase by the subscript g. The global density equation is written as follow:

$$\rho = \alpha\rho_g + (1-\alpha)\rho_l. \tag{1}$$

Where α, the void fraction, is equal to 0 when the cell contains only liquid, 1 when the cell contains only gas, and in between when the cell contains both gas and liquid. The void fraction is transported indirectly. The species transport equation solves the species mass fraction in the cell:

$$\frac{\partial\rho_m}{\partial t} + \frac{\partial\rho_m u_j}{\partial x_j} = \frac{\partial}{\partial x_j}\left(\rho D\frac{\partial Y_m}{\partial x_j}\right), m = 1\dots n \tag{2}$$

with $\rho_m = Y_m\rho$ being the density of the species m, Y_m its mass fraction and n is the total number of species. D is the diffusion coefficient. The total mass of gas (m_g) in the cell is calculated and the mass of liquid (m_l) can be deducted knowing $m_l = 1 - m_g$ and $m_g = \sum_{m=1}^{n_g} Y_m$ with n_g as the number of gas species. Finally, the void fraction is calculated with:

$$\alpha = \frac{m_g}{\rho_g}\left(\frac{m_g}{\rho_g} + \frac{m_l}{\rho_l}\right)^{-1}. \tag{3}$$

2.2. Cavitation model

Cavitation is here modeled using the flash-boiling hypothesis of Shields et al. (Shields et al., 2011). The mass exchange between vapor and liquid is modeled by describing the rate at which the mass fraction of vapor (Y_v) in a two-phase mixture approaches its equilibrium value. The rate follows the equation by Bilicki and Kestin (Bilicki and Kestin, 1990):

$$\frac{DY_v}{Dt} = \frac{\bar{Y_v} - Y_v}{\theta} \tag{4}$$

with Y_v being the instantaneous mass, $\bar{Y_v}$ the equilibrium mass and θ the time scale over which Y_v relaxes to $\bar{Y_v}$ (Richards et al., 2017). $\bar{Y_v}$ is a function of the local enthalpy:

$$\bar{Y_v} = \frac{h - h_l}{h_v - h_l} \tag{5}$$

and the time scale for evaporation is defined as (Downar-Zapolski et al., 1996) :

$$\theta = 3.84.10^{-7}\alpha^{-0.54}\phi^{-1.76} \tag{6}$$

with ϕ as the non dimensional pressure ratio:

$$\phi = \frac{P_{\text{sat}} - P}{P_{\text{crit}} - P_{\text{sat}}}. \tag{7}$$

Here P_{sat} and P_{crit} are the saturation pressure and the critical pressure respectively. The ideal gas equation of state is used to couple density, pressure and temperature of the vapor phase:

$$\frac{P}{\rho} = \frac{RT}{W} \tag{8}$$

with R as the universal gas constant and W the molecular weight of the gas. The pressure below which ammonia becomes gaseous at the range of temperature studied is low enough for the ideal gas law to be sufficiently accurate in this study.

2.3. Domain description

The geometry of the 6 holes counter bore injector is shown in Fig. 1. The nozzle holes have a diameter of 227 µm and a counter bore diameter of 453 µm as determined following the technique in (Macian et al., 2003).

At the inlet, liquid ammonia at a temperature of 300 K and a pressure of 200 bar enters the domain. At the outlet, a

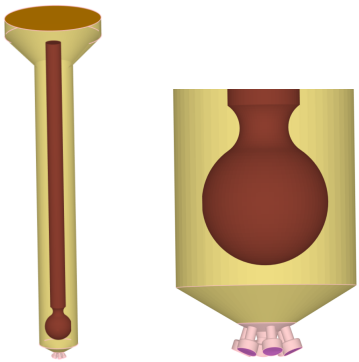

(a) (b)

Figure 1: Geometry of the simulated injector: full injector and zoom on the nozzle head.

pressure of 1 bar and a temperature of 300 K is imposed. Liquid ammonia is specified in case of backflow. The rest of the domain is composed of walls following the law-of-the-wall boundary condition for velocity, and the heat transfer model is set to O'Rourke and Amsden (Amsden, 1997). The needle inside the injector is a moving wall with a translating motion up and down. The needle movement mimics open and closed conditions during which the fuel is either injected or not injected into the engine. As common in numerical simulation, the injector cannot be entirely shut by resting the needle directly against the nozzle seat. The minimum needle lift is here defined with 2e-4 mm and a numerical separation between the two volumes. A secondary region at the bottom of the nozzle is defined in order to capture this (see Fig. 1b). When the needle is at its minimal lift, the injector is considered closed, and no flow travels between the region, and when the needle lifts again, the injection starts, and the flow travels between the region.

2.4. Grid convergence

A grid convergence study is carried out with a base grid of 110 µm, 70 µm, and 50 µm. Details about the setup are presented in Table 1. The mesh for a slice in the middle of the domain is shown in Fig. 2.

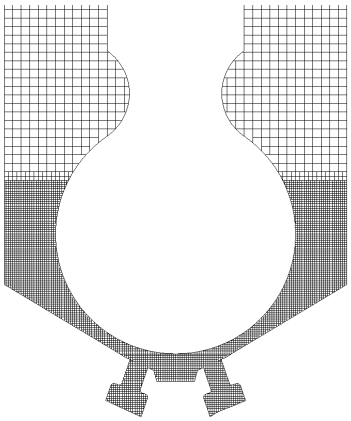

Figure 2: Mesh of the nozzle head.

Figure 3 shows the comparison of the three meshes' influence on the mass flow rate at the outlet. The normalized lift profile is also plotted. Mass flow rate is selected for the grid convergence study here. The internal flow distribution may require further grid refinement, which would be relevant to study for spray injection, but this is outside this work's scope.

Table 1: Comparison of mesh convergence.

	Coarse	Medium	Fine
Base mesh size [µm]	110	70	50
Average time step [s]	3.97e-8	3.25e-8	7.27e-8
Peak cell count [cells]	2e6	2.1e6	4.8e6

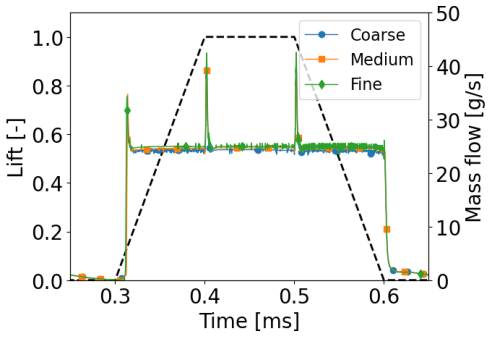

Figure 3: Comparison of the liquid ammonia flow rate during injection from the three meshes: coarse, medium and fine. The normalized lift profile is also plotted.

The results indicate accurate numerical prognosis for the three meshes. Oscillations seem to be diminished with the finer mesh but are reasonable for the other meshes. Going forward, the base grid of 70 μm is selected to study the results.

3. Results and discussion

3.1. Reference case : Ammonia at 300K

The reference case is as described in the domain description : liquid ammonia at 300 K is injected at 200 bar at the inlet, the outlet is set to 1 bar, the wall temperature is at 300 K. The mass flow rate, discharge coefficient and temperature evolution during the fuel's injection are investigated hereafter.

3.1.1. Mass flow rate during injection

Figure 3 shows the total mass flow rate through the 6 holes. When the needle reaches its final lifted position at 0.4 ms, a jump in mass flow rate injection is seen, then again at 0.5 ms when the needle starts to move down again. This is linked to a pressure surge that occurs as the needle stops in its trajectory, and then again when it starts to move from its idle position. This pressure jump, shown Fig. 4 is a numerical artefact, linked to the simulated movement of the needle in the injector. The fuel at the inflow is injected at a pressure of 200 bar, but as can be seen in Fig. 4, the average outflow pressure during the injection is around 40 bar due to the pressure losses in the injector and cavitation effect. The shown pressure is an average of the liquid and vapor pressure at the outlet. In future studies it would be interesting to evaluate the partial pressures of vapor and liquid, and also identify pressure losses due to friction.

3.1.2. Discharge coefficient

One of the objectives of this paper is to identify the discharge coefficient, a coefficient comprised between 0 and 1 that is an indication of how smoothly the flow

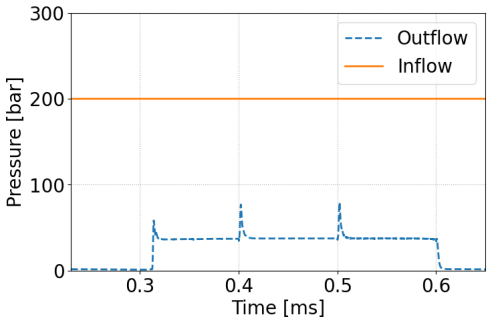

Figure 4: Time evolution of the pressure during injection at the inlet and the outlet.

passes through an orifice. This information can then be used as input for Lagrangian spray simulations or 0-D modeling. The discharge coefficient C_d is defined as the ratio between the theoretical ideal liquid mass flow rate through the outlet and the actual liquid mass flow rate. The theoretical liquid mass flow rate is determined using the following formula based on Bernoulli equation:

$$\dot{m}_{ideal} = A\sqrt{2\rho\Delta P} \tag{9}$$

with A being the nozzle outlet area, ρ the inlet density, and ΔP the difference between the upstream and downstream pressure. The discharge coefficient is defined as:

$$C_d = \frac{\dot{m}_{real}}{\dot{m}_{ideal}} \tag{10}$$

with $\dot{m}_{real}$ as the computed mass flow rate of liquid ammonia through the outlet.
To obtain the liquid mass flow rate, the fraction of liquid at the outlet can be computed using the averaged density at the outlet, as well as the density of gaseous ammonia (10 kg/m^3) and liquid ammonia (600 kg/m^3):

$$\rho_{avg} = X_g\rho_g + X_l\rho_l \tag{11}$$

with

$$X_l + X_g = 1. \tag{12}$$

The resulting liquid fraction of ammonia is shown in Fig. 5, comparing the outflow and inflow liquid fraction. A significant reduction of the liquid fraction is predicted inside the injector, from a fully liquid fuel at the inlet to only 20% of liquid fuel remaining at the outlet. This indicates a significant degree of cavitation that has to be taken into account when studying ammonia sprays in practical systems.
Finally, a liquid discharge coefficient of less than 0.05 is computed, as seen Fig. 6. This is a very low value, and is likely due to the shape of the injector, especially the impact of the counter bore that is causing cavitation, vaporizing the fuel inside the nozzle.
Figure 7 shows the void fraction during the fuel injection when the injected flow has reached steady-state corresponding to Fig. 5. Here it is noticeable that vapor is starting to form when the flow enters the nozzle, caused, among other things, by the sharp edge of the orifices. As the flow interacts with the counter bore, more vapor is formed due to the area expansion. Indeed, the nozzle geometry causes the flow to accelerate (Fig. 8 and Fig. 9). The strong acceleration causes a pressure drop in the nozzle as seen in Fig. 10 due to the high kinetic energy of the fuel. When the pressure is below the

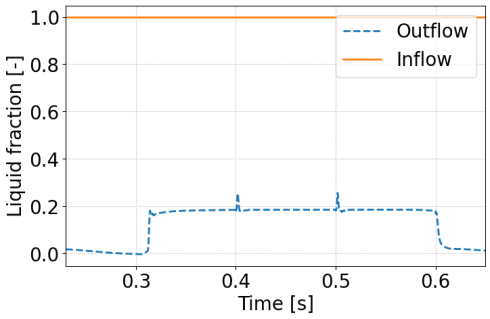

Figure 5: Time evolution of the fraction of liquid during injection at the inlet and the outlet.

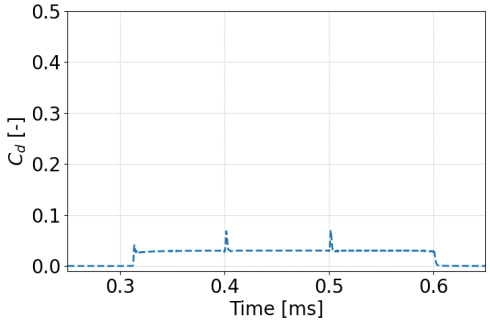

Figure 6: Time evolution of the discharge coefficient at the outlet during injection.

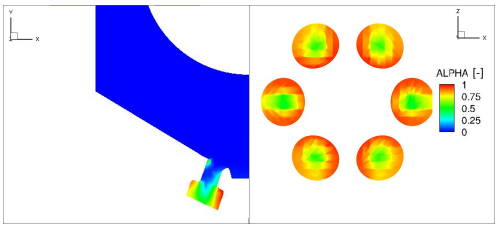

Figure 7: Contours of void fraction at steady state condition.

saturation pressure at the given temperature, the phase change occurs. This is observed here in the nozzles as the pressure drops below 11 bar at 300 K.

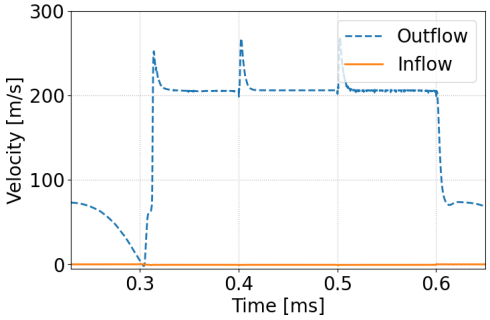

Figure 8: Average velocity at the outlet during the injection.

3.1.3. Temperature evolution during the injection
The average temperature at the inlet of the injector and its outlet during the injection is shown in Fig. 11. This

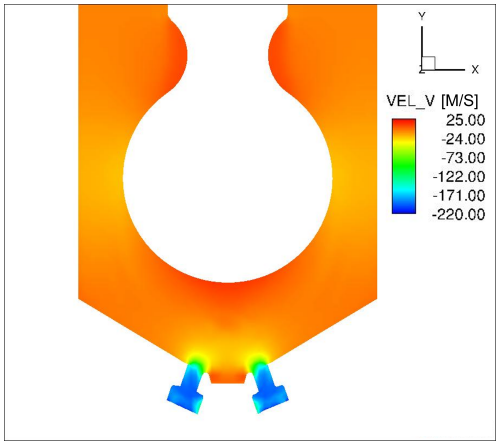

Figure 9: Contour of velocity component v at steady state condition (the values are negative due to the axis orientation).

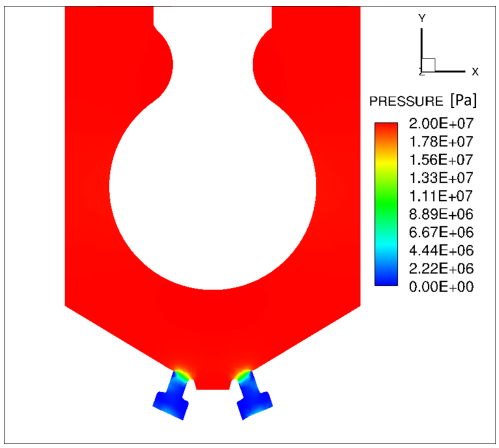

Figure 10: Contour of pressure at steady state condition.

plot shows the average contributions of both the vapor and the liquid phase. Before the start of injection ($t < 0.3$ ms), the fuel at the outlet is fully vaporized. The velocity (Fig. 8) indicates that the gas is slowing down due to its expansion in the nozzle counter bore. This is because the flow is subsonic as seen in Fig. 12. The gas undergoing expansion cools down, explaining the temperature drop to almost 270 K. This can be explained by the positive Joule-Thomson coefficient at 300 K that describes the cooling of gaseous ammonia during expansion (Beattie, 1930). During the injection ($0.3 > t > 0.6$ ms), the liquid fuel undergoes phase change with the liquid fuel in the injector vaporizing. Energy from the fuel is lost to the system during the phase change with latent heat exchanged with the boundaries such as the walls. The injected fuel's temperature therefore remains below the inlet temperature. Figure 13 compares the fuel's heat and kinetic energy. The negative heat illustrates that energy from the fuel is lost to the system. Despite this, vapor formation still occur due to the pressure drop caused by the increased kinetic energy of the fuel, as explained in the previous section.

3.2. Influence of the fuel : Comparison with iso-octane

An additional simulation is set up with iso-octane to compare ammonia's behavior to a traditional fuel in the same injector. Iso-octane is a surrogate for gasoline, a well-known fuel used in engines, notably in direct injection (Zhuang et al., 2017). Because iso-octane will

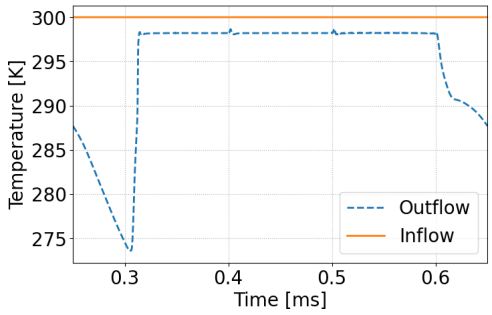

Figure 11: Time evolution of the temperature during injection at the inlet and the outlet.

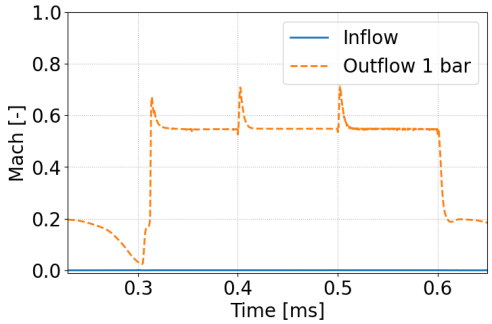

Figure 12: Time evolution of Mach number during injection at the inlet and the outlet.

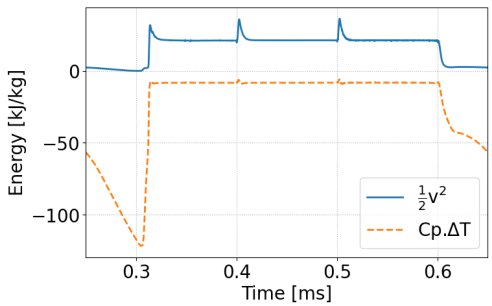

Figure 13: Energy evolution at the outlet during the injection.

not undergo phase change at the given pressure range at 300 K, the temperature is raised to 500 K in this simulations (see Fig. 14). Comparing the two fuels allows the evaluation of the fuel's property's influence on the injection process. Figure 15 shows the time evolution during the injection for both ammonia and iso-octane. A higher liquid fraction of fuel is found at the outlet for ammonia, resulting in a higher liquid discharge coefficient. Despite similar saturation pressure for the two fuels at the operating temperature, the saturation heat of vaporization of iso-octane is lower at the present study's temperature (Fig. 16). This can be the reason for higher vapor generation for iso-octane at the given temperature since less energy from the boundary is needed to vaporize the fuel. Furthermore, it seems based on Fig. 17 that more kinetic energy is provided to the fuel, likely due to iso-octane's lower viscosity that makes it flow faster than ammonia. This higher kinetic energy then cause higher vapor formation. This confirms that the injector's geometry and its counter bore are not the sole responsible for cavitation generation and that the fuel's property and boundaries have a strong influence.

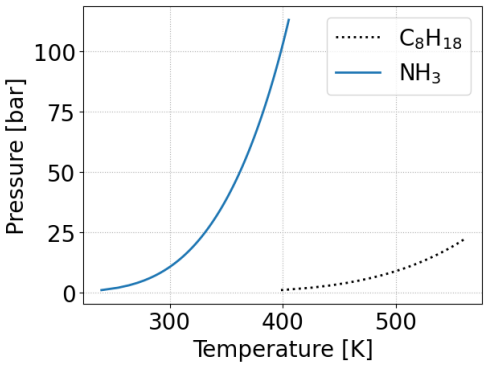

Figure 14: Liquid-vapor curve for ammonia and iso-octane: below the saturation curve, the fuel is gaseous, above it is liquid.

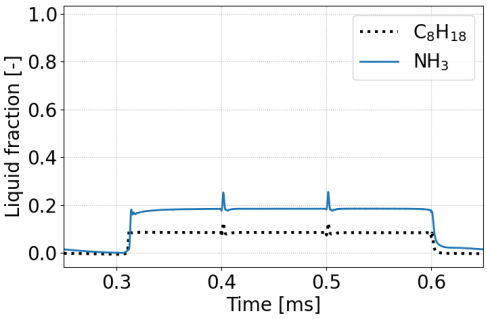

Figure 15: Time evolution of the fraction of liquid during injection at the outlet for ammonia and iso-octane.

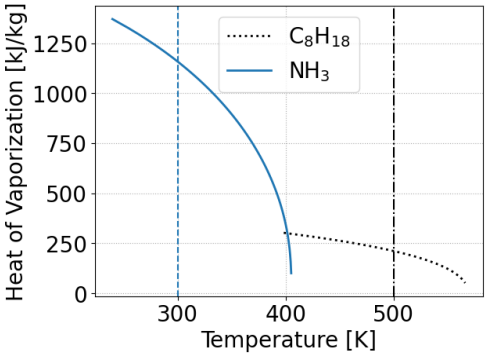

Figure 16: Heat of vaporization saturation curve for ammonia and iso-octane. The vertical lines indicate the temperature of the fuels in the present study (300 K for ammonia, 500 K for iso-octane).

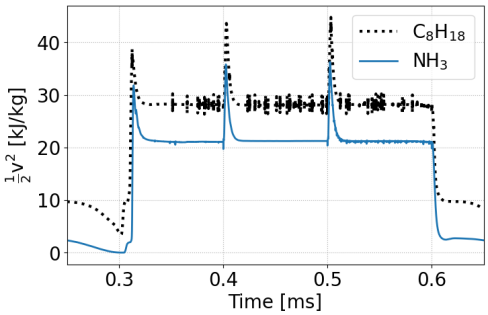

Figure 17: Time evolution of kinetic energy during injection at the outlet for ammonia and iso-octane.

3.3. Influence of the outlet condition: Pressure

Other parameters at the outlet need to be investigated to get more realistic engine conditions. The study at 1 bar shows that there was no backflow of fuel in the injector, therefore, the specified temperature at the outlet will not be investigated further in this study. The wall temperature can have an impact as it would be heating the fuel and will be investigated in the next section. In this section, the pressure at the outlet is modified to imitate the pressure in an engine. Figure 18 shows the liquid discharge coefficient at different outlet pressures. As the outlet pressure increases, the discharge coefficient is increased. Indeed, since the pressure difference between the inlet and the outlet is smaller, the velocity decreases, the proportion of liquid at the outlet is higher and therefore the predicted cavitation is lower (Fig. 19 and Fig. 20). At an outlet pressure of 40 bar, almost none of the fuel has vaporized. The surrounding conditions and especially the pressure difference drives the velocity of the flow across the nozzle and dictates whether or not cavitation will occur. In (Saha et al., 2017), liquid fraction between 0.4 and 0.5 was found when injecting iso-octane pressurized at 200 bar in a chamber at 6 bar. In our case, at 5 bar the liquid fraction is between 0.3 and 0.4, a similar order of magnitude. The difference in value can be linked to the nature of the fuel used and the different geometries.

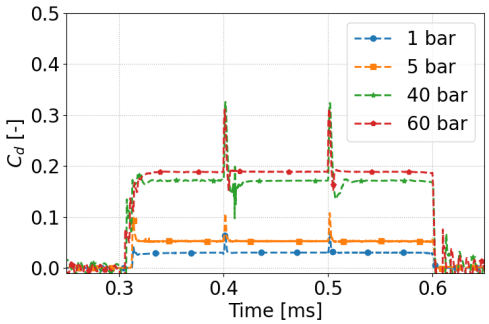

Figure 18: Time evolution of discharge coefficients during injection for different outlet pressures.

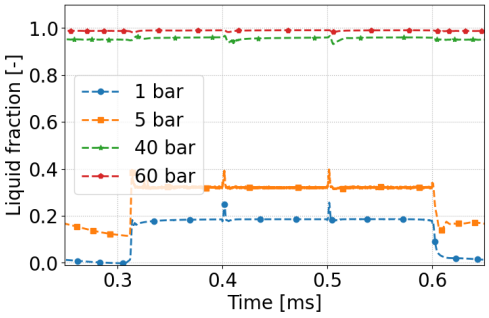

Figure 19: Time evolution of fraction of liquid at the outlet during injection for different outlet pressures.

3.4. Influence of the boundary condition: Wall temperature

To assess the impact of the heat transfer on the fluid, the wall temperature of the nozzle is varied. The outlet pressure is kept the same as the reference study at 1 bar to isolate the effect of the heat transfer. Figure 21 shows the liquid fraction of the fuel during the injection with different wall temperatures imposed: 300 K, 400

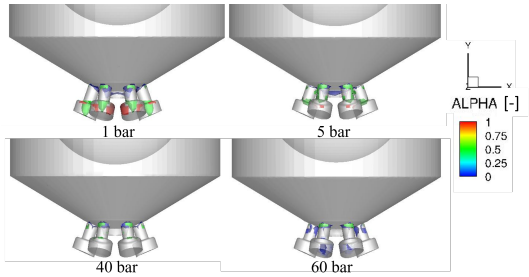

Figure 20: Contour of the void fraction during injection for different outlet pressures at 3.7 ms.

K and 600 K. As the wall temperature increases, energy is provided to the fuel as illustrated Fig. 22, the fuel temperature also increases as expected. The kinetic energy however remains the same for all cases. When the wall temperature is at 300 K, the fluid looses energy to the system, and the kinetic energy only causes vapor formation. However, for the wall temperature of 400 K and 600 K, positive values of heat shows that energy coming from the wall is provided to the fuel. This causes the fuel to further vaporize.

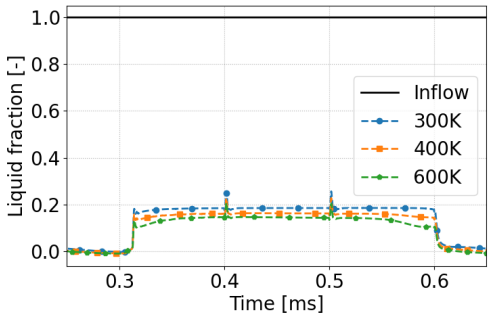

Figure 21: Time evolution of fluid liquid fraction during injection at the inlet and at the outlet for different wall temperature.

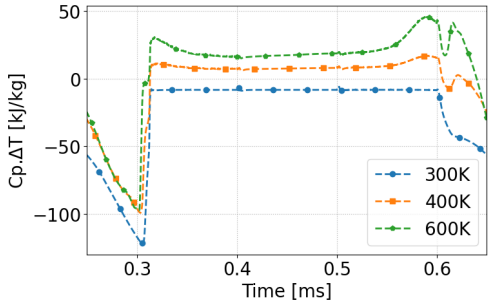

Figure 22: Time evolution of the fuel's heat during injection at the outlet for different wall temperature.

4. Conclusion

3-D RANS simulations were performed using CONVERGE CFD to study the internal flow of a 6-holes injector. Two energy sources seem to cause vapor formation : heat provided to the fuel from the boundary, and kinetic energy causing a pressure drop below the saturation pressure. This study first showed the impact of the nozzle geometry on the vapor formation of ammonia: the sharp edges in this given geometry (based on a real commercialized injector) accelerate the flow causing a pressure drop. When the pressure drops below the saturation pressure, vaporization of the liquid fuel occurs. The presence of the counter bore inducing an expansion causes the gaseous fuel to cool down due to the Joule-Thomson effect. The amount of fuel vaporizing depends not only on the geometry, but also on the outlet conditions, and especially the pressure at the outlet. Higher pressure at the outlet will decrease the fuel vaporization and improve the discharge coefficient of the nozzle. At engine-relevant condition, the discharge coefficient is typically around 0.2. Furthermore, it is found that the wall's temperature affect the amount of fuel cavitating, which is increased with increased wall temperature.

The fuel's properties also impact the amount of cavitation. Fuels with high saturation pressure will cavitate more than fuels with lower saturation pressures. Furthermore, the fuel's viscosity impact the velocity of the flow and hence the cavitation amount.

This study shows that it is indeed possible to adapt to ammonia fuel in ICE with possibly minor changes to the injector design. More work will be needed in the future to understand the cavitation of ammonia in more detail and in different injector's geometry. Coupling of in-nozzle flow with Lagrangian spray simulations will provide further information on ammonia spray formation before computing reacting flows in full engines simulations.

Acknowledgment

The Authors gratefully acknowledge the support from the Norwegian Research Council and related partners in the Low Emission Centre. The computations were performed on resources provided by Sigma2 - the National Infrastructure for High Performance Computing and Data Storage in Norway as well as on the IDUN cluster at the Norwegian University of Science and Technology. Convergent Science provided CONVERGE licenses and technical support for this work.

References

Amsden, A. (1997), 'Kiva-3v: A block-structured kiva program for engines with vertical or canted valves'. doi: 10.2172/505339.
URL: *https://doi.org/10.2172/505339*

Beattie, J. A. (1930), 'A simple equation for the joule-thomson effect in real gases', *Physical Review* **35**, 643. doi: 10.1103/PhysRev.35.643.
URL: *https://journals.aps.org/pr/abstract/10.1103/PhysRev.35.643*

Bilicki, Z. and Kestin, J. (1990), 'Physical aspects of the relaxation model in two-phase flow', *Proceedings of the Royal Society of London. A. Mathematical and Physical Sciences* (1875), 379–397. doi: 10.1098/rspa.1990.0040.
URL: *https://doi.org/10.1098/rspa.1990.0040*

Cheng, Q., Ojanen, K., Diao, Y., Kaario, O. and Larmi, M. (2022), 'Dynamics of the ammonia spray using high-speed schlieren imaging', *SAE Technical Paper* . doi: 10.4271/2022-01-0053.
URL: *https://doi.org/10.4271/2022-01-0053*

Downar-Zapolski, P., Bilicki, Z., Bolle, L. and Franco, J. (1996), 'The non-equilibrium relaxation model for one-dimensional flashing liquid flow', *International Journal of Multiphase Flow* pp. 473–483. doi: 10.1016/0301-9322(95)00078-X.
URL: *https://doi.org/10.1016/0301-9322(95)00078-X*

Lhuillier, C., Brequigny, P., Contino, F. and Mounaïm-Rousselle, C. (2020), 'Experimental study on ammonia/hydrogen/air combustion in spark ignition engine conditions', *Fuel* . doi:

10.1016/J.FUEL.2020.117448.
URL: *https://doi.org/10.1016/j.fuel.2020.117448*

Macian, V., Bermúdez, V., Payri, R. and Gimeno, J. (2003), 'New technique for determination of internal geometry of a diesel nozzle with the use of silicone methodology', *Experimental Techniques* pp. 39–43. doi: 10.1111/j.1747-1567.2003.tb00107.x.
URL: *https://doi.org/10.1111/j.1747-1567.2003.tb00107.x*

Mounaïm-Rousselle, C., Bréquigny, P., Dumand, C. and Houillé, S. (2021), 'Operating limits for ammonia fuel spark-ignition engine'. doi: 10.3390/en14144141.
URL: *https://doi.org/10.3390/en14144141*

Mounaïm-Rousselle, C., Bréquigny, P., Medina, A. V., Boulet, E., Emberson, D. and Løvås, T. (2022), 'Ammonia as fuel for transportation to mitigate zero carbon impact', *Energy, Environment, and Sustainability* pp. 257–279. doi: 10.1007/978-981-16-8717-4_11.
URL: *https://link.springer.com/chapter/10.1007/978-981-16-8717-4_11*

Niki, Y., Yoo, D.-H., Hirata, K. and Sekiguchi, H. (2016), 'Effects of ammonia gas mixed into intake air on combustion and emissions characteristics in diesel engine'. doi: 10.1115/ICEF2016-9364.
URL: *http://asmedigitalcollection.asme.org/ICEF/proceedings-pdf/ICEF2016/50503/V001T03A004/2443686/v001t03a004-icef2016-9364.pdf*

Pelé, R., Mounaïm-Rousselle, C., Bréquigny, P., Hespel, C., Bellettre, J., Begg, S. and Emekwuru, N. (2021), 'First study on ammonia spray characteristics with a current gdi engine injector', *Fuels 2021, Vol. 2, Pages 253-271* pp. 253–271. doi: 10.3390/fuels2030015.
URL: *https://doi.org/10.3390/fuels2030015*

Reiter, A. J. and Kong, S. C. (2008), 'Demonstration of compression-ignition engine combustion using ammonia in reducing greenhouse gas emissions', *Energy and Fuels* **22**, 2963–2971. doi: 10.1021/ef800140f.
URL: *https://doi.org/10.1021/ef800140f*

Richards, K. J., Senecal, P. K. and Pomraning, E. (2017), *CONVERGE Manual v3.0*.

Saha, K., Quan, S., Battistoni, M., Som, S., Senecal, P. K. and Pomraning, E. (2017), 'Coupled eulerian internal nozzle flow and lagrangian spray simulations for gdi systems', *SAE Technical Papers* . doi: 10.4271/2017-01-0834.
URL: *https://doi.org/10.4271/2017-01-0834*

Serras-Pereira, J., Romunde, Z. V., Aleiferis, P. G., Richardson, D., Wallace, S. and Cracknell, R. F. (2010), 'Cavitation, primary break-up and flash boiling of gasoline, iso-octane and n-pentane with a real-size optical direct-injection nozzle', *Fuel* **89**, 2592–2607. doi: 10.1016/J.FUEL.2010.03.030.
URL: *https://doi.org/10.1016/j.fuel.2010.03.030*

Shields, B., Neroorkar, K. and Schmidt, D. P. (2011), 'Cavitation as rapid flash boiling', *ILASS-Americas 23rd Annual Conference on Liquid Atomization and Spray Systems, Ventura, CA, May 2011* .
URL: *http://refhub.elsevier.com/S0017-9310(21)00036-3/sbref0038*

Torelli, R., Som, S., Pei, Y., Zhang, Y., Voice, A., Traver, M. and Cleary, D. (2017), 'Comparison of in-nozzle flow characteristics of naphtha and n-dodecane fuels', *SAE Technical Papers* . doi: 10.4271/2017-01-0853.
URL: *https://doi.org/10.4271/2017-01-0853*

Wang, C., Xu, H., Herreros, J. M., Wang, J. and Cracknell, R. (2014), 'Impact of fuel and injection system on particle emissions from a gdi engine', *Applied Energy* pp. 178–191. doi: 10.1016/J.APENERGY.2014.06.012.
URL: *http://dx.doi.org/10.1016/j.apenergy.2014.06.012*

Zhuang, Y., Qian, Y. and Hong, G. (2017), 'The effect of ethanol direct injection on knock mitigation in a gasoline port injection engine', *Fuel* pp. 187–197. doi: 10.1016/J.FUEL.2017.08.060.
URL: *https://doi.org/10.1016/j.fuel.2017.08.060*